Helical α-Synuclein Forms Highly Conductive Ion Channels†

Stanislav D. Zakharov,‡,§ John D. Hulleman,|| Elena A. Dutseva,⊥ Yuri N. Antonenko,⊥ Jean-Christophe Rochet,*,|| and William A. Cramer*,‡

Departments of Biological Sciences and Medicinal Chemistry and Molecular Pharmacology, Purdue University, West Lafayette, Indiana 47907-2054, Institute of Basic Biological Problems, Russian Academy of Sciences, Puschino, Moscow Region 140290, Russian Federation, and A. N. Belozersky Institute of Physico-Chemical Biology, Moscow State University, Moscow 119992, Russian Federation

Received June 28, 2007; Revised Manuscript Received October 9, 2007

ABSTRACT: α-Synuclein (αS) is a cytosolic protein involved in the etiology of Parkinson's disease (PD). Disordered in an aqueous environment, αS develops a highly helical conformation when bound to membranes having a negatively charged surface and a large curvature. It exhibits a membrane-permeabilizing activity that has been attributed to oligomeric protofibrillar forms. In this study, monomeric wild-type αS and two mutants associated with familial PD, E46K and A53T, formed ion channels with well-defined conductance states in membranes containing 25−50% anionic lipid and 50% phosphatidylethanolamine (PE) in the presence of a trans-negative potential. Another familial mutant, A30P, known to have a lower membrane affinity, did not form ion channels. Ca^{2+} prevented channel formation when added to membranes before αS and decreased channel conductance when added to preformed channels. In contrast to the monomer, membrane permeabilization by oligomeric αS was not characterized by formation of discrete channels, a requirement for PE lipid, or a membrane potential. Channel activity, α-helical content, thermal stability of membrane-bound αS determined by far-UV CD, and lateral mobility of αS bound to planar membranes measured by fluorescence correlation spectroscopy were correlated. It was inferred that discrete ion channels with well-defined conductance states were formed in the presence of a membrane potential by one or several molecules of monomeric αS in an α-helical conformation and that such channels may have a role in the normal function and/or pathophysiology of the protein.

α-Synuclein (αS),[1] a 140 residue cytosolic protein enriched in neurons, is involved in the pathogenesis of Parkinson's disease (PD) (*1*). Membrane binding is thought to be essential for the cellular function of αS, which may involve regulation of the size of a reserve pool of synaptic vesicles in the brain (*1*, *2*). Disordered in an aqueous environment, monomeric αS develops an α-helical conformation upon binding to membranes containing anionic lipid or phosphatidylethanolamine (PE), a phospholipid that supports nonbilayer structures, or when it is bound to the curved membranes of vesicles with a small diameter (*3*−*5*).

An NMR structure obtained in the presence of the anionic detergent SDS (*6*−*8*) revealed two long α-helices separated by a turn in the N-terminal and central regions of αS. The segment spanning residues 4−60 has a basic character (p*I* 9.5; Figure 1). The C-terminal region of αS (residues 104−140) is very acidic (p*I* 3.1) and therefore would have a limited interaction with a negatively charged membrane surface. Three point mutants of αS linked to familial PD, A30P, E46K, and A53T, have different membrane-binding affinities. A30P and E46K have lower and higher affinity than wild-type αS, and the affinity of A53T is similar to that of wild-type αS (*5*, *9*−*14*).

During fibrillization, αS forms oligomeric intermediates termed protofibrils (*15*, *16*). It has been shown that protofibrillar αS and other soluble amyloid oligomers bind strongly to vesicle membranes and form porelike structures with nonselective leakage of compounds having a hydrodynamic radius less than ∼2.5 nm (*17*−*21*). Membrane permeabilization by αS protofibrils has been considered to be a ubiquitous example of the action of an amyloid pore, which has been proposed to underlie a mechanism common to neurodegenerative disease pathogenesis (*19*−*22*). An alternative proposal for a porelike mechanism of membrane permeabilization is that soluble amyloid oligomers do not form discrete ion channels but rather increase membrane conductance by decreasing the membrane dielectric barrier (*22*, *23*). It is noteworthy that previously described liposome

† Financial support for these studies was provided by NIH Grants GM-18457 (W.A.C.), NS-049221 (J.-C.R.), and Fogarty TW01235 (Y.N.A. and W.A.C.).

* Corresponding authors: (W.A.C.) phone 765-494-4956, fax 765-496-1189, e-mail waclab@purdue.edu; (J.-C.R.) phone 765-494-1413; e-mail rochet@pharmacy.purdue.edu.

‡ Department of Biological Sciences, Purdue University.

§ Russian Academy of Sciences.

|| Department of Medicinal Chemistry and Molecular Pharmacology, Purdue University.

⊥ Moscow State University.

[1] Abbreviations: αS, α-synuclein; CD, circular dichroism; DO, dioleoyl; FCS, fluorescence correlation spectroscopy; FFT, fast Fourier transform; FPLC, fast protein liquid chromatography; HEPES, *N*-(2-hydroxyethyl)piperazine-*N*′-ethanesulfonic acid; LUV, large unilamellar vesicles; NAC, non-Aβ component of AD amyloid; NMR, nuclear magnetic resonance; PC, PE, PG, and PS, phosphatidylcholine, -ethanolamine, -glycerol, and -serine; PD, Parkinson's disease; SUV, small unilamellar vesicles; T_m, midpoint temperature of thermal melting transition; TMR, tetramethylrhodamine-6-maleimide.

10.1021/bi701275p CCC: $37.00
Published on Web 11/22/2007

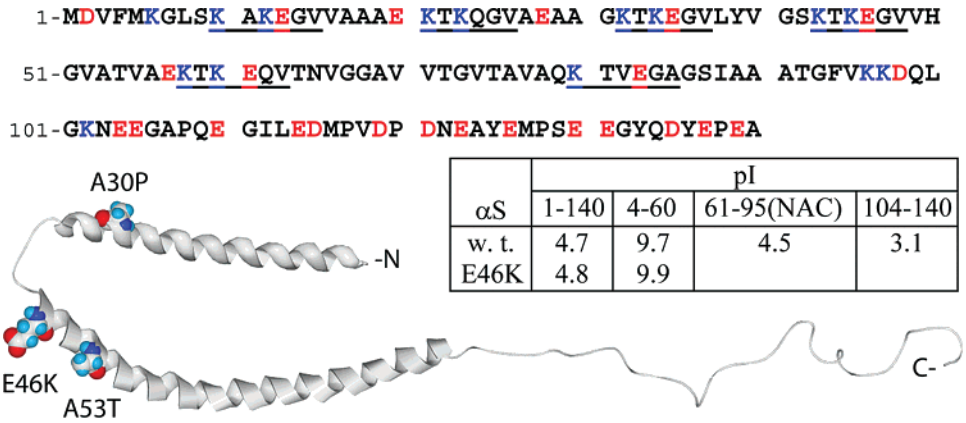

αS	pI 1-140	4-60	61-95(NAC)	104-140
w. t.	4.7	9.7	4.5	3.1
E46K	4.8	9.9		

FIGURE 1: Amino acid sequence and distribution of p*I* values of αS; ribbon diagram derived from NMR structure of α-synuclein bound to SDS micelles [PDB code 1XQ8 (*8*)]. Acidic (D, E) and basic (K, R) side chains are shown in red and blue in the sequence, in which six imperfect hexamer repeats are highlighted. Table: isoelectric points (p*I*) of full-length αS, residues 1−140, and its N-terminal basic (4−60), central NAC (61−95), and C-terminal acidic (104−140) segments, were calculated with the program ProtParam (*25*). Ribbon diagram of αS and position of mutations A30P, E46K, and A53T, associated with PD familial mutants, were generated by Swiss-PDB viewer version 3.7 and POV-ray version 3.6 programs.

permeabilization by oligomeric αS required the presence of anionic lipid and was more efficient with SUV of 30 nm diameter than with LUV, properties similar to those demonstrated for helix formation by monomeric αS (*17*, *18*).

In this study, monomeric wild-type αS and the E46K and A53T mutants related to familial PD were shown to form ion channels in planar bilayer membranes containing anionic and curvature-inducing lipids. From the correlation between the lipid specificity for formation of discrete ion channels and the helical secondary structure, as well as from FCS analysis of lateral mobility of αS in the planar bilayer membrane, it was concluded that well-defined stable ion channels can be formed by monomeric αS in an α-helical conformation.

EXPERIMENTAL PROCEDURES

Purification of Recombinant α-Synuclein. Recombinant αS was expressed in *Escherichia coli* and purified as described previously (*16*, *24*). After ammonium sulfate precipitation, the redissolved protein mixture was boiled for 5 min, cleared of insoluble protein by centrifugation and filtration (0.22 μm filter), and purified on a DEAE-Sepharose FF column (16 × 100 mm, Amersham Biosciences). Fractions containing αS, identified by SDS−PAGE, were dialyzed against 10 mM NH_4HCO_3 and lyophilized. A solution of αS was prepared by dissolving the lyophilized protein in 20 mM NaP_i, pH 7.4, to a concentration of 0.3−1 mM. Monomeric, dimeric, and oligomeric αS were isolated by fractionating the dissolved protein on a Superdex 200 column, as described previously (*16*). The αS concentration was determined after subtraction of background light scattering by use of the extinction coefficient 5960 M^{-1} cm^{-1} at 280 nm (*25*).

Fluorescent Labeling of αS. The monomeric A53C mutant of αS, 0.2 mM, was incubated with tetramethylrhodamine-6-maleimide (TMR), 1 mM, at 4 °C for 10 h. Free TMR was removed by size-exclusion chromatography on a Sephadex G-25 column.

Vesicle Preparation. Phospholipids DOPC, DOPE, DOPG, and DOPS were purchased from Avanti Polar Lipids (Alabaster, AL). LUV were prepared as decribed (*26*) by extrusion through a polycarbonate filter with 0.1 μm pores. SUV were prepared by ultrasonic treatment of lipid suspension in buffer solution in an ultrasonic bath (Bransonic 12, Branson).

Circular Dichroism. Far-UV CD spectral measurements were carried out with a J-810 spectropolarimeter (Jasco). Spectra were measured at 25 °C, in cuvettes with an optical path length of 0.1 mm. The fractional helix content of αS, $H_{\alpha S}$, was calculated as previously described (*27*), with the assumption of linear dependence on the measured mean molar ellipticity at 222 nm, Θ_{222}:

$$H_{\alpha S} = \frac{\Theta_{222} - \Theta_{aq}}{\Theta_{max}\left(1 - \frac{x}{N_r}\right) - \Theta_{aq}} \quad (1)$$

where Θ_{aq} = 2680 deg cm^2 $dmol^{-1}$ is the mean molar ellipticity of unordered αS in an aqueous environment, and Θ_{max} = −42 500 deg cm^2 $dmol^{-1}$ is the ellipticity of a complete helix of infinite length. The correction for end effects, $1 - (x/N_r)$, is associated with x non-hydrogen-bonded carbonyls in a complete helix. For αS, N_r = 140 amino acids and x = 3 (*27*).

Thermal denaturation of membrane-bound αS was measured at 222 nm in a stirred cuvette with an optical path length of 5 mm and a rate of temperature change of 0.5 °C/min. The apparent midpoint temperature of the protein melting transition, T_m, was obtained from the first derivative of the thermal melting curve after noise reduction via a FFT algorithm.

Fluorescence Correlation Spectroscopy. Experiments were carried out on free-standing Müller−Rudin-type horizontal planar bilayer lipid membranes (*28*) formed from DOPG and bacterial PE (1:1 by weight; Sigma) by spreading a lipid solution across a circular hole, 0.2 mm in diameter, in a diaphragm separating two aqueous phases. The experimental chamber consisted of a 2 mL lower solution with a 50 μm distance from the bottom glass slide to the septum holding the membrane, and a 0.5 mL upper solution as described (*29*). Formation of a black membrane was observed visually in both transparent and fluorescent modes. The bathing solution contained 100 mM KCl and 2 mM HEPES, pH 7.0. Excitation of fluoresence utilized a Nd:YAG solid-state laser

with a 532 nm beam attached to an Olympus IMT-2 epifluorescent inverted microscope equipped with a 40×, NA 1.2 water immersion objective (Carl Zeiss, Jena, Germany). The fluorescence, after passing through an appropriate dichroic beam splitter and a long-pass filter, was imaged onto a 100 μm core fiber coupled to an avalanche photodiode (SPCM-AQR-13-FC, Perkin-Elmer Optoelectronics, Vaudreuil, Quebec, Canada), whose output signal was digitized with the interface card (Flex02-01D/C, Bridgewater, NJ). The data acquisition time was 30 s. To calibrate the setup, the FCS signal from a solution of rhodamine 6G was recorded. Assuming the diffusion coefficient of the dye to be 2.5×10^{-6} cm^2/s, a value of confocal radius $\omega = 0.61$ μm was obtained. The correlated fluorescence emission signals were fit by a two-dimensional autocorrelation function (*30*):

$$G(\tau) = \frac{1}{N}\frac{1}{1+\frac{\tau}{\tau_D}} \quad (2)$$

where τ and τ_D, respectively, are the time variable and the lateral diffusion time that a molecule stays in the focal volume, and N is the number of particles in this volume. The diffusion coefficient, D, was calculated from the equation for two-dimensional diffusion:

$$D = \frac{\omega^2}{4\tau_D} \quad (3)$$

where ω^2 is the mean square distance that the fluorophore moves in time, τ_D.

Ion Channel Measurements in Planar Bilayers. Planar bilayer membranes were formed as described previously (*31*), by use of an *n*-decane solution of a lipid mixture containing PC, PE, PG, and PS (all dioleoyl forms), at a given molar ratio, applied by a brush technique (*28*), and a bathing solution consisting of 2 mM HEPES and 0.1 M KCl, pH 7.0. αS was added to the cis compartment to a final concentration of 2−10 μg/mL, and the solution was stirred until channels appeared. Trans-membrane current was measured in the voltage-clamp mode with Ag/AgCl electrodes, using a BC-525C amplifier (Warner Instruments, Hamden, CT). The sign of the trans-membrane potential refers to that applied on the cis side of the membrane.

RESULTS

Separation of Aggregated (Oligomeric) and Monomeric Forms of α-Synuclein by FPLC. Lyophilized E46K αS, in an amount (25 mg) sufficient to prepare samples of monomer and oligomer for spectral and channel measurements, was passed through a Superdex 200 column (Figure 2, —). Oligomeric αS eluted in the void column volume (peak at 7.4 mL). The presence of oligomeric αS in the void-volume fraction was verified by Western blotting, which revealed a characteristic smear of αS immunoreactivity in the upper part of the SDS−polyacrylamide gel (*32*). Due to column overloading, the monomeric form eluted as a broad peak between 12.5 and 16.5 mL. An additional peak at 11.5 mL was attributed to small aggregates (dimer). Reruns of dimer/monomer fractions through the same column show the presence of two species that eluted at volumes >11 mL:

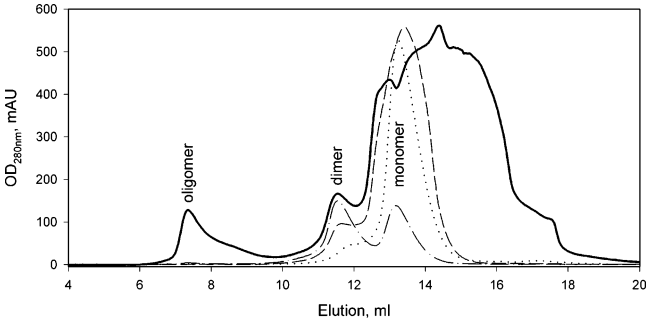

FIGURE 2: Chromatographic separation of oligomeric and monomeric forms of αS. Lyophilized E46K mutant of αS (25 mg) was dissolved in 0.5 mL of 20 mM NaP_i, pH 7.4. After removal of insoluble material by filtration through a 0.2 μm filter, αS was applied to a Superdex 200 column (10/300) with detection of protein peaks by UV absorbance at 280 nm (—). Eluted fractions were concentrated with a 30 kDa cutoff filter and rerun through the same column. Identity of fractions from first column: (i) 7.0−8.0 mL, oligomer (rerun not shown); (ii) 11.0−12.5 mL, dimer (— · —); (iii) 12.5−15.0 mL, monomer (— — —); (iv) 15.0−17.0 mL, which was part of an overloaded region in the first run, eluted as monomer in the second run (· · ·). Elution solution was 20 mM NaP_i, pH 7.4.

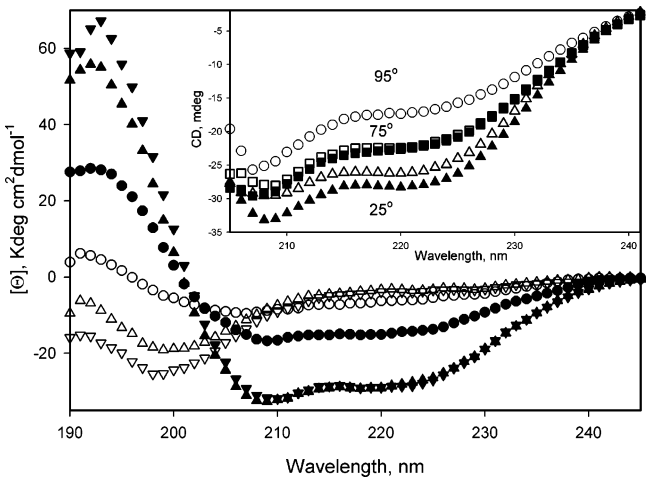

FIGURE 3: Far-UV CD spectra of oligomeric, dimeric, and monomeric αS in solution and bound to SUV containing anionic lipids and PE: spectra of oligomeric (circles), dimeric (triangles), and monomeric (inverted triangles) E46K αS in solution (open symbols) and bound to the membrane surface of SUV that have 50% DOPG/50% DOPE lipid content (solid symbols). Lipid:αS molar ratio was 250:1. (Inset) Refolding of oligomeric αS after thermal melting at 95 °C results in the same or increased helix content. CD spectra of oligomeric E46K αS in the presence of SUV were measured at 25 (△), 55 (not shown), 75 (□) and 95 °C (○), and upon cooling down at 75 (■), 55 (not shown), and 25 °C (▲); 5 min time interval allowed for temperature equilibration between recordings of spectra. Optical path length, 1 mm; 10 μM αS; SUV, 2.5 mM total lipid content.

dimeric (peak 11.5 mL; Figure 2, — · —) and monomeric (peak 13.3 ± 0.2 mL; — — — and ···) αS.

Both dimeric and monomeric αS in solution displayed the far-UV CD spectrum of a completely unordered protein, characterized by a minimum below 200 nm (Figure 3, △). However, in the presence of SUV composed of 50% anionic DOPG and 50% DOPE (Figure 3, ▲), these forms assumed a predominantly helical conformation characterized by minima at 208 and 222 nm and a maximum at 192 nm. Interpretation of the small-amplitude CD spectrum of the soluble oligomer is complicated by the presence of significant

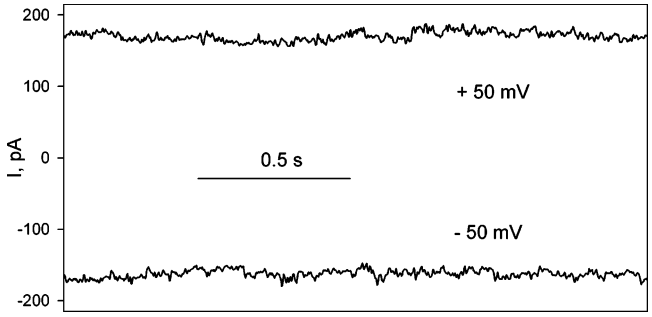

FIGURE 4: Membrane permeabilization by oligomeric E46K αS. Trans-membrane current through planar membrane bilayers was measured at +50 and −50 mV. αS (2 μg/mL) was added to the cis compartment. Oligomeric αS selected from leading fractions was eluted from a size-exclusion column (Figure 2). Bilayer membrane contained 100% DOPG, a concentration at which oligomer is known to be active (*17*), and monomer to be inactive (see below). Bathing solution in this and all bilayer experiments was 2 mM HEPES, pH 7.0, and 0.1 M KCl.

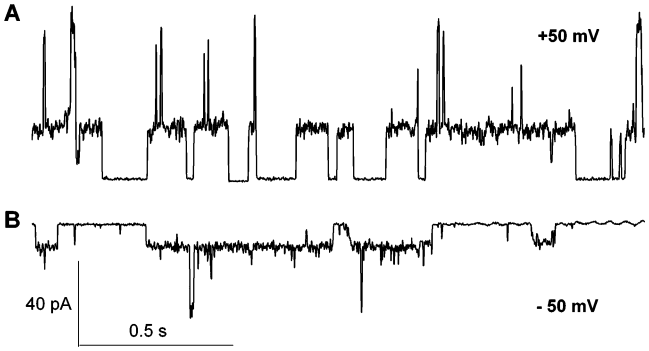

FIGURE 5: Ion channels of αS formed upon application of a trans-negative potential. (A) Trans-membrane current measured under voltage-clamp conditions upon application of trans-membrane potential of +50 mV (trans-negative). (B) Trans-membrane current measured at −50 mV (trans-positive). The membrane contained 50% DOPG and 50% DOPE. Wild-type αS, 8 μg/mL final concentration, was added to the cis compartment with stirring for 20 min before recording.

spectral distortion due to light scattering (Figure 3, ○). In the presence of SUV, a significant increase in helical content could be inferred (Figure 3, ●). Similar CD spectral changes were found for oligomers of wild-type αS (not shown). The finding that the helical content of oligomeric αS increases in the presence of SUV could imply the presence of a fraction of αS oligomers that are able to dissociate to monomeric species upon binding to curved and negatively charged SUV membranes. An estimate of the size of this fraction, based on changes in the amplitude of the CD signal at 222 nm, indicates that it could comprise 30−35% of the oligomer. The thermal melting of membrane-bound oligomeric αS at 95 °C results in an additional increase in helical content upon subsequent cooling to 25 °C.

Properties of α-Synuclein Ion Channels, Oligomer versus Monomer. αS binding to membranes containing anionic lipid is driven by electrostatic interactions between the basic (p*I* = 9.7) N-terminal segment of the protein (Figure 1) and the negatively charged membrane surface. Such interactions depend on the ionic strength of the ambient solution and are significantly diminished in 1 M KCl, a salt concentration commonly used in planar bilayer channel recording. Therefore, measurements of ion channel activity of αS were conducted in 0.1 M KCl.

Oligomer. Oligomeric αS did not induce ion conductivity across membranes formed without anionic lipid. In a membrane made with 100% anionic lipid, DOPG, oligomers induced unstable trans-membrane currents of approximately the same magnitude at both positive and negative trans-membrane potentials (Figure 4). The membrane-permeabilizing activity of the oligomer decreased with lower anionic lipid content and, unlike monomeric αS, did not depend on the presence of PE in the membrane (data not shown), and did not decrease at a trans-positive potential (Figure 4).

Monomer. Monomeric αS (wild type, E46K, and A53T), separated from the oligomer fraction by size-exclusion chromatography, was added to the cis compartment of the planar bilayer membrane (50 mol % PG, 50 mol % PE). In the presence of a potential of +50 mV (trans-side negative), channels with defined conductance states were observed (Figure 5A). A switch to a cis-side negative potential resulted in decreased channel activity (Figure 5B).

Monomeric αS produced ion channels in membranes containing an optimum anionic lipid content. Channels formed relatively rapidly in membranes containing 50 mol % PG but more slowly with 25% or 75% PG, and not at all in membranes consisting of 0 or 100% PG (data not shown). Such channels were also formed in membranes containing phosphatidylserine (PS) as the anionic lipid instead of PG, emphasizing the importance of the net negative charge of the lipid head group for αS channel formation.

Concentrations of 2−5 μg/mL E46K and A53T in the bathing solution were sufficient for channel formation, whereas a somewhat larger concentration (5−10 μg/mL) was required for wild-type αS.

Channel Conductance. The conductance of E46K channels did not differ significantly from that of wild-type αS (Figure 6A). Channels exhibited several conductance states with well-defined amplitude in every trial, but the absolute size of the channels varied in different trials. In a representative experiment, the average dwell time of wild-type 400 pS channels was 110 ± 50 ms, whereas the dwell time distribution of E46K channels was broader and its average value was larger (670 ± 460 ms). In addition to the major conductance state (400 ± 100 pS), channels of E46K and wild-type proteins exhibited a larger conductance state (∼1300 pS; Figure 6A). However, because these channels always opened from a "pedestal" of smaller channels, the net conductance of the larger channels was 800−900 pS. A state of small conductance (<100 pS) was also observed in some trials.

The study of the voltage dependence of αS channels is complicated due to opening of new channels at potentials >80 mV. In a representative trial, where E46K channels were opened upon application of trans-negative potential of −50 mV with 150 and 520 pS conductance states, subsequent measurement of the voltage dependence (20−80 mV) of channel conductance showed an increase in the conductance amplitude. It increased gradually from 140 ± 20 to 280 ± 30 pS and from 420 ± 40 to 580 ± 50 pS for smaller and larger conductance states, respectively (Figure 6A, inset).

PE Requirement. In the absence of PE, the channel activity was reduced, and conductance states were poorly defined. Thus, in membranes composed of 50% PG and 50% PC,

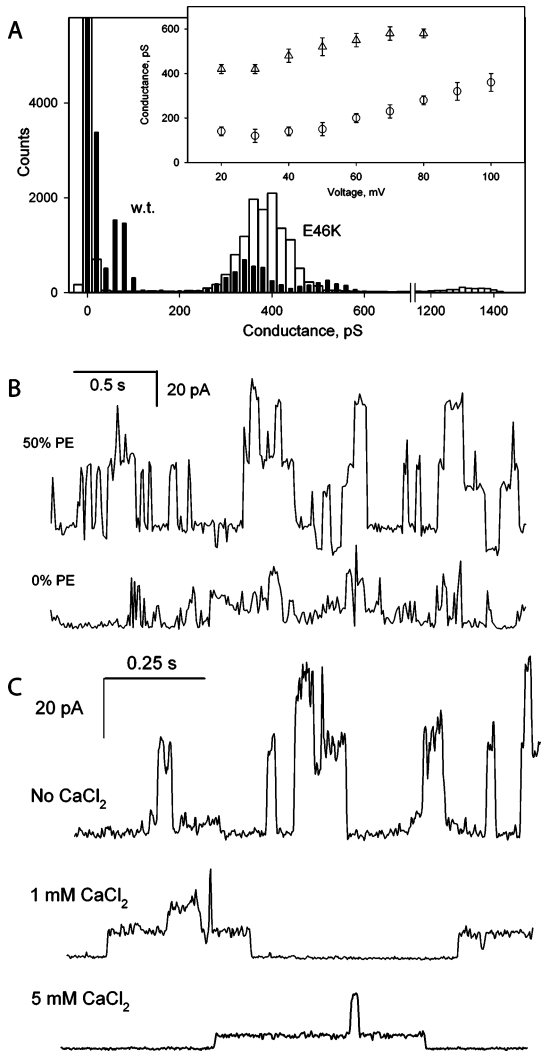

FIGURE 6: Channel properties of αS channels. (A) Histograms of conductance states of wild-type (solid bars) and E46K (open bars) channels (7.5 μg/mL) in the membrane with 50% PG and 50% PE. (Inset) Voltage dependence of conductance of small (○) and large (△) E46K αS channels. The planar membrane was made of an equimolar lipid mixture of DOPG/DOPE. E46K αS, 5 μg/mL. (B) Single-channel traces of E46K αS (5 μg/mL) in planar bilayers with 50% PG/50% PE (top) and 50% PG/50% PC (bottom). Trans-membrane potential was +50 mV (cis). (C) Calcium decreases ion channel conductance of αS. Single-channel traces of A53T mutant at 0 (upper), 1 (middle), and 5 mM (bottom) $CaCl_2$ are shown. Trans-membrane potential was +50 mV. A53T αS (4 μg/mL) was incubated with membrane containing 50% DOPS and 50% DOPE; $CaCl_2$ was added after channel activation. Application of 100 mV potential was required to open channels after incubation with 1 mM $CaCl_2$; 150 mV potential was used to reopen channels in 5 mM $CaCl_2$.

the frequency of appearance of open channels of E46K αS was decreased (Figure 6B). In these membranes, wild-type αS had a channel activity smaller than that of E46K, which was manifested as rare short-lived spikes of variable amplitude (data not shown).

A30P Does Not Form Channels. At the concentrations used for wild-type αS, the monomeric A30P mutant, which is known to have a lower affinity for membranes than wild-type αS and E46K (*12*), did not form ion channels in membranes containing 50% PG in the presence or absence of PE (not shown). Increasing the concentration of A30P αS to >30 μg/mL in the bathing solution resulted in membrane breakage.

Effect of Ca^{2+} on Channel Formation by αS. Ca^{2+} has a crucial role in synaptic transmission and has been shown to bind to the αS acidic C-terminal tail (*33*, *34*). $CaCl_2$ (1 or 5 mM) added from the cis side (but not from the trans side) closed active αS channels. Application of a large potential (≥100 mV) was necessary to reopen channels. However, the size of these channels was significantly smaller (Figure 6C). The channel conductance decreased from 460 ± 80 pS in the absence of Ca^{2+} to 200 ± 40 and 120 ± 20 pS in the presence of 1 or 5 mM $CaCl_2$. When 5 mM $CaCl_2$ was added before αS, channels were not formed even upon application of a large (+150 mV) potential (not shown). Thus, Ca^{2+} ions exerted two different effects on αS channel activity: (i) prevention of channel opening and (ii) decreasing channel conductance of preformed channels. The first effect can be associated with a decrease of membrane surface potential on the cis side of membrane, caused by electrostatic interaction of Ca^{2+} with the membrane surface [for PG and PS membranes, the Ca^{2+}-binding constant = 17 and 26.5 M^{-1}, respectively (*35*)]. The Gouy−Chapman−Stern formalism predicts an approximately 27 and 40 mV decrease in the surface potential of a membrane containing 50% anionic lipid at 0.1 M ionic strength in the presence of 1 and 5 mM $CaCl_2$ (*36*). The Ca^{2+}-induced decrease in conductance of preformed channels may be associated with the direct interaction of Ca^{2+} with αS, possibly with the acidic C-terminal tail (*33*, *34*), implying a role of the C-terminal region in regulation of αS channels.

α-Helicity of Membrane-Bound α-Synuclein. The lipid dependence of the secondary structure of membrane-bound αS was compared to that of the channel-forming activity, via far-UV CD spectral analysis of membrane vesicles in the same solution as was used for channel measurements. LUV [diameter 100−140 nm (*37*)] were used instead of small vesicles, as the former are less stressed mechanically (*5*), so that their mechanical properties resemble more closely those of planar bilayer membranes.

Far-UV CD spectra of αS bound to LUV were measured at a lipid/αS molar ratio of 250:1 (Figure 7A). The spectra documented an increase in α-helical content of E46K and wild-type αS with increasing content of anionic PG lipid (Figure 7A) and of PE in the presence of 25 mol % PG (Figure 7A, inset). The position of an isosbestic point at 204 ± 1 nm for each set of spectra implies that the αS secondary structure undergoes a direct transition from an unordered to an α-helical conformation (*38*). In 0.1 M KCl, the helix content of wild-type and E46K αS increased from ∼20% in LUV with 25% PG/75% PC to 66% in LUV with 75% PG/25% PC (Table 1). An increase in the partial content of PE in membranes with 25 mol % PG resulted in an increase in the α-helical content from ∼20% in the absence of PE to 45−50% in membranes with 75% PE (Table 1). The A30P mutant also displayed an increase in helix content with increasing anionic lipid concentration and increasing content of PE, but its helicity was markedly smaller (Table 1).

In the presence of $CaCl_2$ (1 mM), the helix content of wild-type αS, bound to LUV (50% PG/50% PE), was ∼17% smaller, independent of the sequence of addition of $CaCl_2$ and αS to LUV (Table 1). This is believed to be a

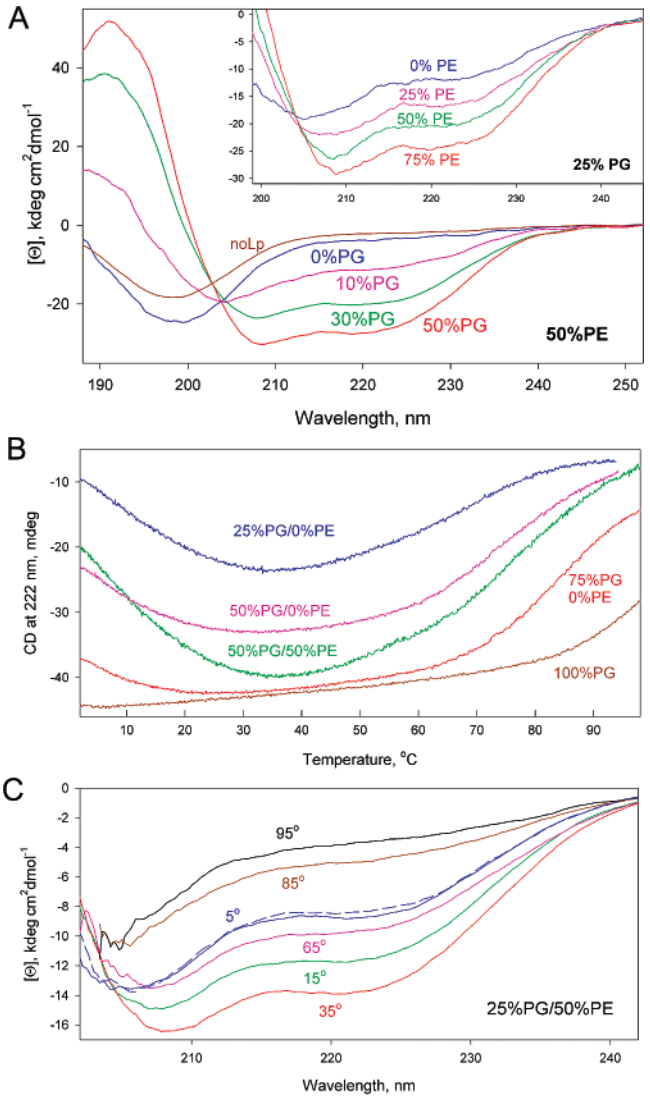

FIGURE 7: Circular dichroic analysis of secondary structure and thermal stability of αS in LUV as a function of partial content of DOPG and DOPE. (A) Far-UV CD spectra of E46K αS (10 μM) bound to LUV (2.5 mM total lipid) at 25 °C. Lipid composition (DOPG/DOPE/DOPC, mol %) of LUV: 0/50/50 (blue), 10/50/40 (pink), 30/50/20 (green), 50/50/0 (red), and absence of LUV (brown).(Inset) CD spectra of wild-type αS (16 μM) in the presence of LUV (4 mM total lipid). Lipid composition: 25/0/75 (blue), 25/25/50 (pink), 25/50/25 (green), and 25/75/0 (red). NoLp, no lipid. (B) Thermal scans of CD signal at 220 nm of αS bound to LUV (DOPG/DOPE/DOPC, mol %): 25/0/75 (blue), 50/0/50 (pink), 50/50/0 (green), 75/0/25 (red), and 100/0/0 (brown). For better presentation, some curves are vertically offset. (C) CD spectra of wild-type αS (4 μM) bound to LUV (1 mM total lipid; 25% PG/50% PE) measured at temperatures increasing from 5 to 95 °C: 5 (blue, solid), 15 (green), 35 (red), 65 (pink), 80 (brown), and 95 °C (black), and 5 °C after cooling from 95 °C (blue, dashed). Equilibration time between measurements of spectra, 5 min; optical path length, 1 mm; buffer, 5 mM NaP_i and 0.1 M KCl, pH 7.0.

consequence of a decrease of the membrane surface potential (*35*, *39*), as discussed above.

Thus, αS bound to membranes with a lipid composition optimal for channel formation (50% PG/50% PE) has a predominantly helical secondary structure (ca. 65%; 91 residues). The A30P mutant of αS bound to these vesicles is 47% helical (62 residues), similar to the helix content of wild-type αS and E46K bound to membranes with 25% PG/50% PE, in which they form ion channels. This implies that the inability of A30P to form channels is not associated with an insufficient content of α-helix but is more likely due to an absence of local helicity around Pro30.

Thermal Melting Analysis of Liposome-Bound αS. The thermal stability of the α-helical structure of αS in the membrane-bound state was studied by far-UV CD spectra and continuous registration at 222 nm of the amplitude of the CD signal, as a function of temperature (0−98 °C). From the melting curves, the apparent melting temperature, T_m, can be calculated from the first derivative of the melting curve function whose maximum corresponds to the T_m of thermal unfolding. The T_m was used to determine the thermal stability of αS as a function of the content of PG and PE lipid (Table 1).

The amplitude of the far-UV circular dichroism signal at 222 nm of wild-type αS bound to membranes containing 50% PG and 50% PE increases monotonically with increasing temperature from 0 to 35−40 °C, reaching a maximum at ∼37 °C (Figure 7B, green). CD spectra document that the helicity of αS increases significantly in this temperature range (Figure 7C), implying that membrane-bound αS undergoes cold denaturation below ∼35 °C. In the temperature range 40−98 °C, the magnitude of the CD signal at 222 nm and the far-UV CD spectra show a gradual decrease in the helical content of αS (T_m ∼75 °C), resulting in almost complete unfolding at 95 °C (Figure 7B,C). Melting of αS helices is reversible, as can be seen from restoration of the CD spectra after cooling down to 5 °C (Figure 7C, blue).

The thermal stability of membrane-bound αS increases with increasing anionic lipid content, measured as the fraction of the CD signal lost at 2 °C relative to the maximum amplitude of the CD signal at approximately 35 °C (Table 1; Figure 7B). The decrease in signal amplitude at 2 °C relative to 35 °C is small at 75% PG, in comparison with 50% PG, and is not seen with 100% PG (Figure 7B). The stability of the A30P helical structure is markedly lower than that of wild-type and E46K αS, as inferred from a lower T_m and larger extent of cold denaturation (Table 1). The decrease in αS helix stability with decreasing temperature below 30 °C implies involvement of hydrophobic interactions in helix stabilization (*40*) and correlates with the mechanical stress effect imposed by PE on the membrane bilayer. It is hypothesized that α-helices of membrane-bound αS are presumably inserted deeper into the interfacial layer of the membrane in the presence of PE. Imposition of a membrane potential would cause movement of these helices to a transmembrane orientation that allows channel formation.

Fluorescence Correlation Spectroscopy of αS Bound to Planar Bilayer Membranes. While the majority of studies on membrane interactions of αS attributed its membrane-permeabilization ability exclusively to the β-structure-rich oligomeric form of αS, it was inferred from the studies described above that α-helical αS added to the membrane as a monomer can form highly conductive ion channels. The question arises as to whether αS remains monomeric and α-helical after it is bound to planar bilayer membranes. Additional insight regarding the monomeric versus oligomeric state of αS in planar bilayer membranes was sought through fluorescence correlation spectroscopy (FCS), for which αS(A53C) was labeled with the fluorescent probe TMR and added to the upper compartment of a planar membrane apparatus. Autocorrelation of the fluorescence

Table 1: α-Helix Content and Midpoint of Thermal Unfolding of αS Bound to LUV as a Function of Anionic Lipid and PE[a]

lipid, mol %		helix, %			T_m, °C (cold denaturation, %)		
PG	PE	wt	E46K	A30P	wt	E46K	A30P
10	0	4 ± 2	4 ± 3	0	nd[b]	nd	nd
10	50	13 ± 2	15 ± 4	0	nd	nd	nd
10	75	16 ± 5	15 ± 2	3	nd	nd	nd
25	0	18 ± 7	20 ± 9	4 ± 3	66 ± 4 (56)	70 (54)	nd
25	25	34 ± 5	31 ± 2	10 ± 5	70 ± 1 (56)	70 ± 2 (64)	nd
25	50	41 ± 7	38 ± 5	15 ± 5	73 ± 1 (56)	75 (52)	<70 (100)
25	75	49 ± 7	45 ± 6	20 ± 7	73 ± 1 (53)	74 ± 3 (58)	65.0 (91)
50	0	62 ± 9	57 ± 7	37 ± 5	74 ± 1 (35)	79 (25)	69 ± 2 (52)
50	50	67 ± 8	63 ± 4	47 ± 7	80 ± 1 (30)	90 ± 2 (15)	72 ± 2 (47)
+Ca[c]	50	50 ± 6	nd	nd	89 ± 2 (33)	nd	nd
75	0	66 ± 8	66 ± 4	51 ± 11	85 ± 1 (15)	≥88 (8)	81 (31)
100	0	71 ± 8	76 ± 3	55 ± 10	>90 (8)	>93 (3)	≥89 (14)

[a] Wild-type and mutant αS were mixed with LUV at an αS/lipid molar ratio of 1:250. Buffer was 2 mM HEPES, pH 7.0, and 0.1 M KCl. Helix content was determined by CD analysis at 25 °C as described under Experimental Procedures. Thermal denaturation was measured at 220 nm from 0 to 98 °C with a thermal scanning rate of 30 °C/h. αS and LUV were mixed at room temperature and incubated on ice for 5 h before the start of the thermal scan. The cold denaturation effect is presented as the fraction of the magnitude of the CD signal at 2 °C relative to the maximum amplitude detected in a given thermal scan, $100(\Theta_{max} - \Theta_{2°})/\Theta_{max}$. Mean and standard deviation values are based on results of 3−5 measurements of α-helix content and 2−3 measurements of thermal denaturation parameters. [b] Not determined. [c] Wild-type αS bound to LUV (50% PG/50% PE) in the presence of 1 mM $CaCl_2$; sequence of addition to LUV of αS and $CaCl_2$ did not affect helix content of αS.

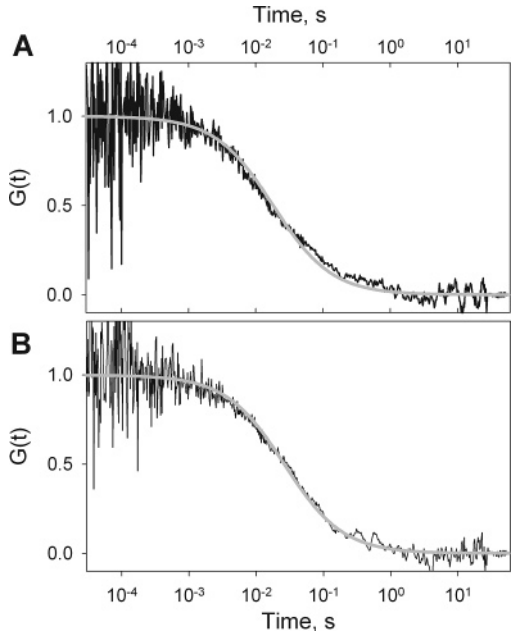

FIGURE 8: FCS analysis of lateral mobility of αS in planar bilayer membranes. (A) FCS measurements of TMR-labeled A53C αS bound to a horizontal planar bilayer lipid membrane made of DOPG and bacterial PE lipid (1:1 by weight). Autocorrelation function (eq 2) with $\tau_D = 18$ ms, fit to the data, is shown in gray. (B) FCS measurement with rhodamine-labeled PE fit to an autocorrelation function with $\tau_D = 26$ ms.

emission of membrane-bound protein (Figure 8A) was described by eq 2 with average diffusion time $\tau_D = 16 \pm 3$ ms, which led to a calculated diffusion coefficient of 5.8 ± 1.2 $\mu m^2/s$. This diffusion coefficient was compared to that of rhodamine-labeled lipid (PE) in a membrane with the same lipid composition (Figure 8B). The fit of eq 2 to the data yielded a value of $\tau_D = 26$ ms, similar to the τ_D of the protein. The average diffusion coefficient was 3.9 ± 0.5 $\mu m^2/s$, which is similar to that (3 $\mu m^2/s$), measured previously by FCS for lipid diffusion in giant vesicles (*41*). The small difference might arise from a difference in phospholipid composition. Because the membrane diffusion coefficient is dependent on the size of the diffusing particle, the similarity of the lateral diffusion coefficients of αS and lipid in the membrane implies an absence of higher order oligomers in the membrane-bound αS. These data confirm the assignment of the channel activity of αS measured in planar bilayer membranes to protein initially adsorbed to the membrane in a monomeric state, from which active channels are formed in the presence of a trans-negative potential.

DISCUSSION

The major conclusion of this study is that one or several membrane-bound monomeric αS in an α-helical conformation (Figure 9A) can form discrete highly conductive channels in the presence of a trans-membrane potential (Figure 9B).

Several previously reported observations imply that the ion channels observed in the current studies are formed by helical αS and do not result from the presence of small undetectable amounts of β-sheet-rich protofibrils: (i) A30P lacks channel activity, consistent with the diminished helicity of this variant in the presence of vesicles compared to wild-type αS (*9*, *11*, *12*). In contrast, protofibrillar A30P exhibits a higher membrane permeabilization activity than protofibrils formed from the wild-type protein (*18*). (ii) Helical E46K αS forms channels with longer dwell times than wild-type αS, whereas a recent report indicated that protofibrillar E46K has a significantly decreased permeabilizing activity compared to wild-type protofibrils (*14*). (iii) Ca^{2+} ions significantly reduced the conductance of preopened helical αS channels (Figure 6C) and prevented channel formation when it was added before αS. In contrast, membrane permeabilization by the protofibrils was detected in the presence of 5 mM $CaCl_2$ (*17*, *18*).

Direct Unordered-to-Helix Structure Transition of α-Synuclein upon Membrane Binding. CD spectral analysis revealed the direct unordered-to-helical structure transition in αS upon binding to LUV (Figure 7A). The helix content increased with an increase in surface charge of the membranes and in the presence of PE. These previously documented effects (*3*−*5*, *9*) are in agreement with the NMR structure of αS in anionic detergent solution (*6*−*8*), which

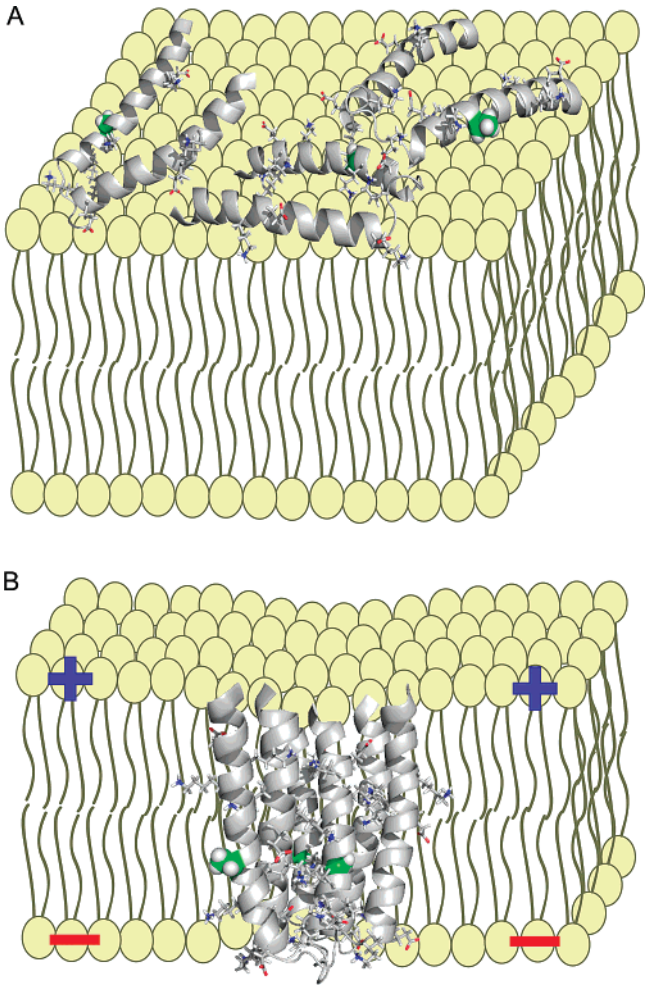

FIGURE 9: Helical hairpin trans-membrane reorientation in electrical field could result in ion channel formation. (A) In the absence of the trans-negative potential, helical hairpins derived from three αS molecules on the interfacial layer of the cis side leaflet of bilayer. (B) Trans-membrane reorientation of three helical hairpins under a trans-negative potential. The number of hairpins needed to form a channel is not known and is proposed to be small, 2−4, provided by 1−4 molecules of αS. Each helical hairpin is modeled by use of atomic coordinates of an αS segment spanning residues 14−68 in the NMR structure [PDB code 1XQ8 (*8*)]. The side chains of four KxKE repeats in this segment are shown as sticks (atoms N and O shown in blue and red, respectively), and Ala30 side chain (green) is shown in space-filling representation.

shows the presence of two long helices separated by a break or turn (Figure 1). Thus, the lipid requirement for helical structure formation is similar to that for the formation by αS of stable highly conductive ion channels (Figures 5 and 6). Two lines of evidence support this conclusion: (i) the far-UV CD analysis of αS bound to liposomes shows the membrane-bound form to be predominantly (∼70%) α-helical. No significant tendency to form oligomers could be found. (ii) FCS analysis of TMR-labeled A53C mutant of αS bound to planar bilayer lipid membranes showed that its mobility is characterized by a diffusion coefficient of 5.8 ± 1.2 $\mu m^2/s$ (Figure 8A), slightly larger than that of individual lipid molecules. Thus, monomeric αS does not aggregate upon binding to the planar bilayer membranes used in the present studies.

A maximum of ∼70% in the helix content of membrane-bound αS (Table 1) would include approximately 98 residues. Assuming that the acidic C-terminal segment, spanning residues 104−140 (Figure 1), is electrostatically repelled from the negatively charged membrane surface, the entire N-terminal (residues 1−60) and central (residues 61−100) segments attain a predominantly helical conformation in the membrane-bound state. The αS helices are characterized by three turns per 11 residues (3/11 helix), rather than the standard α-helix with 5 turns per 18 residues, and have an amphipathic folding pattern (*3*, *7*).

A30P Mutant. The helix content of the A30P mutant was reduced by ∼20% (Table 1), implying that Pro30 prevents helix formation in an approximately 28-residue-long segment of αS. The lower helicity could be caused partly by weaker binding to the liposomes (*12*); however, decreased thermal stability of the membrane-bound A30P (Table 1) implies impairment of the helical structure of αS by the A30P substitution. Comparison of NMR structures of wild-type and A30P αS bound to SDS micelles (*7*, *10*) showed that the A30P substitution causes changes in backbone $^1H^N$ chemical shifts over ±30 residues from the mutation site, which are associated with a helix break between residues Gln24 and Lys32, disturbance of the sequence of hydrophobic and polar residues in the amphiphilic helices, and a significant decrease in bending of the N-terminal helix. The helix break around proline in the A30P mutant and alteration of the amphiphilic order could explain its loss of channel activity, assuming that this segment is moving through the hydrophobic core during channel formation (Figure 9B).

Amphipathic Helices and Channel Formation. The 11-residue periodicity in the N-terminal region with the highly conserved hexamer motif KTKE/QGV makes αS similar to the exchangeable apolipoproteins with lipid-binding class A amphipathic α-helical repeats (*3*). In this class of helices, the nonpolar face is bordered by positively charged residues, and the face containing negatively charged residues is located opposite the nonpolar face. Class A helices of apolipoproteins are involved in solubilization of lipid micelles, and at low concentration they stabilize membranes by affecting the spontaneous membrane curvature (*42*). A similar stabilizing effect of αS on lipid packing in small vesicles, a lipid annealing effect previously described (*5*), suggests that this could be a physiological function of αS (*2*). Amphipathic helical peptides also have pore-forming properties (*43*), which require peptide aggregation in membranes. Such pores could be lined by peptide helices ("barrel-stave" model) or also involve lipids ("toroidal pore" model) (*44*, *45*). A similar mechanism of channel formation was proposed for larger proteins with α-helical bundle structures, such as pore-forming colicins (*31*), apoptotic proteins (*46*), and *Bacillus thuringiensis* toxin (*42*). One molecule of such a protein toxin is sufficient to form a pore with several pairs of antiparallel helices in trans-membrane orientation. In the closed channel state, these helices can form a two-dimensional array in the membrane interfacial layer (*47*).

Channel Formation by Helical α-Synuclein. For monomeric αS, which has a high propensity for amphipathic helix formation, an α-helical conformation of a monomer is thermodynamically more favorable in the membrane-bound state than a β-strand structure (*3*). Upon application of a trans-negative potential, αS helices can move to a trans-membrane orientation as helical hairpins (Figure 9). The basic character of KxKE repeats allows voltage sensing and could serve as energy-transducer elements to drive the helices

into a trans-membrane orientation. Two or three such hairpins, which could be formed by one or several molecules of αS, would be sufficient for ion channel formation (Figure 9). A helix break due to the A30P mutation close to the apex of the helix hairpin would increase the energy cost of this hairpin movement across the hydrophobic core of the membrane.

Lipid Requirement. Electrostatic interactions with the membrane surface are necessary for αS binding and the transition to a helical conformation but are not sufficient to create conditions for a voltage-dependent structural rearrangement. The formation of stable, highly conductive channels requires the presence of PE in the membrane. This lipid with a small headgroup generates intrinsic curvature in the membrane bilayer, changing its elastic properties (*48*, *49*). αS could sense membrane curvature by inserting amphipathic domains between lipid headgroups, releasing mechanical stress generated by the presence of PE. The lack of channel formation in membranes with 100% PG could be explained by the absence of PE in the membrane, and also by especially tight binding to the membrane interfacial layer that prevents voltage-dependent structural rearrangement, as described for the bactericidal pore-forming colicin E1 (*50*).

Physiological Significance. To address the question of the physiological role of ion channel formation by αS, one must account for the following observations: (i) αS is primarily an intracellular protein (some reported exceptions are discussed below); (ii) stable channels are formed in membranes containing PE, which is present in neuronal membranes (*51*, *52*); and (iii) a trans-negative potential is required for channel activity. If the requirement for a trans-negative potential applies in vivo, as in the cell-free system employed in this study, then intracellular αS should form active channels only in membranes that have been depolarized. In neurons, membrane depolarization occurs transiently during an action potential associated with impulse transmission. Accordingly, it can be proposed that intracellular, helical αS may form ion channels in synaptic membranes in response to an action potential. Channel formation may be part of the normal function of αS and could result in modulation of ion movements related to depolarization/repolarization. Mouse knockout studies indicate that αS plays a critical role in regulating neurotransmitter release evoked by action potentials in hippocampal slices (*53*). Membrane depolarization triggers opening of voltage-gated Ca^{2+} channels. The resulting influx of Ca^{2+} in the presynaptic terminal couples the action potential to neurotransmitter release (*54*, *55*). Increased Ca^{2+} levels may thus regulate αS channel activity at the synaptic membrane following membrane depolarization.

Mutants of αS involved in familial PD may elicit neurotoxicity via alteration of intracellular channel activity of αS. The E46K and A53T replacements could induce channel hyperactivity, whereas the A30P substitution apparently suppresses channel formation altogether. Presumably, familial mutants that perturb the function of helical αS channels would be unable to exert normal function or a function in neurodegeneration, and any role of αS in the latter would arise from an alternative pathway involving membrane permeabilization by β-sheet-rich protofibrils (*17*−*22*).

Although αS is located primarily inside the cell, emerging evidence suggests that a portion of the protein resides in the extracellular space, possibly due to secretion and/or cell lysis (*56*−*58*). Conceivably, extracellular αS could form helical channels in membranes at their resting potential (i.e., excess negative charge on the intracellular side), provided that PE is present in the plasma membrane. Ion channel formation by extracellular, helical αS would likely induce cytotoxicity by dissipating the potential across the plasma membrane, similar to the mode of action of bacterial channel-forming toxins such as the colicins (*59*). Channels formed by extracellular αS could target both neuronal and glial cells, thereby inducing neurodegeneration and glial activation associated with PD (*57*, *58*).

The data presented in this study do not necessarily imply that αS-induced cell death involves channel formation exclusively by α-helical αS instead of previously described pathogenic mechanisms such as membrane disruption by β-sheet-rich protofibrils. Rather, it is proposed that the formation of α-helical channels provides an alternative mechanism that contributes to normal function and toxicity of αS both inside the cell and in the extracellular milieu.

REFERENCES

1. Cookson, M. R. (2005) The biochemistry of Parkinson's disease, *Annu. Rev. Biochem. 74*, 29−52.
2. Murphy, D. D., Rueter, S. M., Trojanowsky, J. Q., and Lee, V. M.-Y. (2000) Synucleins are developmentally expressed, and α-synuclein regulates the size of the presynaptic vesicular pool in primary hippocampal neurons, *J. Neurosci. 20*, 3214−3220.
3. Davidson, W. S., Jonas, A., Clayton, D. F., and George, J. M. (1998) Stabilization of α-synuclein secondary structure upon binding to synthetic membranes, *J. Biol. Chem. 273*, 9443−9449.
4. Jo, E., McLaurin, J., Yip, C. M., St. George-Hyslop, P., and Fraser, P. E. (2000) α-Synuclein membrane interactions and lipid specificity, *J. Biol. Chem. 275*, 34328−34334.
5. Nuscher, B., Kamp, F., Mehnert, T., Odoy, S., Haass, C., Kahle, P. J., and Beyer, K. (2004) α-Synuclein has a high affinity for packing defects in a bilayer membrane. A thermodynamics study, *J. Biol. Chem. 279*, 21966−21975.
6. Chandra, S., Chen, X., Rizo, J., Jahn, R., and Sudhof, T. C. (2003) A broken α-helix in folded α-synuclein, *J. Biol. Chem. 278*, 15313−15318.
7. Bussell, J. R., and Eliezer, D. (2003) A structural and functional role for 11-mer repeats in α-synuclein and other exchangeable lipid binding proteins, *J. Mol. Biol. 329*, 763−778.
8. Ulmer, T. S., Bax, A., Cole, N. B., and Nussbaum, R. L. (2005) Structure and dynamics of micelle-bound human α-synuclein, *J. Biol. Chem. 280*, 9595−9603.
9. Perrin, R. J., Woods, W. S., Clayton, D. F., and George, J. M. (2000) Interaction of human α-synuclein and Parkinson's disease variants with phospholipids. Structural analysis using site-directed mutagenesis, *J. Biol. Chem. 275*, 34393−34398.
10. Ulmer, T. S., and Bax, A. (2005) Comparison of structure and dynamics of micelle-bound human α-synuclein and Parkinson disease variants, *J. Biol. Chem. 280*, 43179−43187.
11. Jensen, P. H., Nielsen, M. S., Jakes, R., Dotti, C. G., and Goedert, M. (1998) Binding of α-synuclein to brain vesicles is abolished by familial Parkinson's disease mutation, *J. Biol. Chem. 273*, 26292−26294.
12. Jo, E., Fuller, N., Rand, R. P., St. George-Hyslop, P., and Fraser, L. (2002) Defective membrane interactions of familial Parkinson's disease mutant A30P α-synuclein, *J. Mol. Biol. 315*, 799−807.
13. Choi, W., Zibaee, S., Jakes, R., Serpell, L. C., Davletov, B., Crowther, R. A., and Goedert, M. (2004) Mutation E46K icreases phospholipid binding and assembly into filaments of human α-synuclein, *FEBS Lett. 576*, 363−368.
14. Fredenburg, R. S., Rospigliosi, C., Meray, R. K., Kessler, J. C., Lashuel, H. A., Eliezer, D., and Lansbury, P. T., Jr. (2007) The impact of the E46K mutation on the properties of α-synuclein in its monomeric and oligomeric states, *Biochemistry 46*, 7107−7118.
15. Conway, K. A., Lee, S.-J., Rochet, J.-C., Ding, T. T., Williamson, R. E., and Lansbury, P. T., Jr. (2000) Acceleration of oligomer-

ization, not fibrillization, is a shared property of both α-synuclein mutations linked to early-onset Parkinson's disease: implications for pathogenesis and therapy, *Proc. Natl. Acad. Sci. U.S.A. 97*, 571−576.
16. Rochet, J.-C., Conway, K. A., and Lansbury, P. T., Jr. (2000) Inhibition of fibrillization and accumulation of prefibrillar oligomers in mixtures of human and mouse α-synuclein, *Biochemistry 39*, 10619−10626.
17. Volles, M. J., Lee, S.-J., Rochet, J.-C., Shtilerman, M. D., Ding, T. T., Kessler, J. C., and Lansbury, P. T., Jr. (2001) Vesicle permeabilization by protofibrillar α-synuclein: implications for the pathogenesis and treatment of Parkinson's disease, *Biochemistry 40*, 7812−7819.
18. Volles, M. J., and Lansbury, P. T., Jr. (2002) Vesicle permeabilization by protofibrillar α-synuclein is sensitive to Parkinson's disease-linked mutations and occurs by pore-like mechanism, *Biochemistry 41*, 4595−4602.
19. Ding, T. T., Lee, S.-J., Rochet, J.-C., and Lansbury, P. T., Jr. (2002) Annular α-synuclein protofibrils are produced when spherical protofibrils are incubated in solution or bound to brain-derived membranes, *Biochemistry 41*, 10209−10217.
20. Quist, A., Doudevski, I., Lin, H., Azimova, R., Ng, D., Frangione, B., Kagan, B., Ghiso, J., and Lal, R. (2005) Amyloid ion channels: a common structural link for protein-misfolding disease, *Proc. Natl. Acad. Sci. U.S.A. 102*, 10427−10432.
21. Lashuel, H. A., and Lansbury, P. T., Jr. (2006) Are amyloid disease caused by protein aggregates that mimic bacterial pore-forming toxins, *Q. Rev. Biophys. 39*, 167−202.
22. Kayed, R., Sokolov, Y., Edmonds, B., McIntire, T. M., Milton, S. C., Hall, J. E., and Glabe, C. G. (2004) Permeabilization of lipid bilayers is a common conformation-dependent activity of soluble amyloid oligomers in protein misfolding diseases, *J. Biol. Chem. 279*, 46363−46366.
23. Sokolov, Y., Kozak, J. A., Kayed, R., Chanturia, A., Glabe, C., and Hall, J. E. (2006) Soluble amyloid oligomers increase bilayer conductance by altering dielectric structure, *J. Gen. Physiol. 128*, 637−647.
24. Conway, K. A., Harper, J. D., and Lansbury, P. T., Jr. (2000) Fibrils formed in vitro from α-synuclein and two mutant forms linked to Parkinson's disease are typical amyloid, *Biochemistry 39*, 2552−2563.
25. Gasteiger, E., Hoogland, C., Gattiker, A., Duvaud, S., Wilkins, M. R., Appel, R. D., and A., B. (2005) in *The Proteomics Protocols Handbook* (Walker, J. M., Ed.) pp 571−607, Humana Press, Totowa, NJ.
26. Hope, M. J., Bally, M. B., Webb, G., and Cullis, P. R. (1985) Production of large unilamellar vesicles by a rapid extrusion procedure. Characterization of size distribution, trapped volume and ability to maintain a membrane potential, *Biochim. Biophys. Acta 812*, 55−65.
27. Rohl, C. A., Chakrabartty, A., and Baldwin, R. L. (1996) Helix propagation and N-cap propensities of the amino acids measured in alanine-based peptides in 40 volume percent trifluoroethanol, *Protein Sci. 5*, 2623−2637.
28. Mueller, P., Rudin, D. O., Tien, H. T., and Wescott, W. C. (1962) Reconstitution of cell membrane structure *in vitro* and its transformation into an excitable system, *Nature 194*, 979.
29. Brutyan, R. A., DeMaria, C., and Harris, A. L. (1995) Horizontal 'solvent-free' lipid bimolecular membranes with two-sided access can be formed and facilitate ion channel reconstitution, *Biochim. Biophys. Acta 1236*, 339−344.
30. Schwille, P., Haupts, U., Maiti, S., and Webb, W. W. (1999) Molecular dynamics in living cells observed by fluorescence correlation spectroscopy with one- and two-photon excitation, *Biophys. J. 77*, 2251−2265.
31. Sobko, A. A., Kotova, E. A., Antonenko, Y. N., Zakharov, S. D., and Cramer, W. A. (2006) Lipid dependence of the channel properties of a colicin E1-lipid toroidal pore, *J. Biol. Chem. 281*, 14408−14416.
32. Rochet, J.-C., Outeiro, T. F., Conway, K. A., Ding, T. T., Volles, M. J., Lashuel, H. A., Bieganski, R. M., Lindquist, S. L., and Lansbury, P. T., Jr. (2004) Interactions among α-synuclein, dopamine, and biomembranes: some clues for understanding neurodegeneration in Parkinson's disease, *J. Mol. Neurosci. 23*, 23−34.
33. Nielsen, M. S., Vorum, H., Lindersson, E., and Jensen, P. H. (2001) Ca^{2+} binding to α-synuclein regulates ligand binding and oligomerization, *J. Biol. Chem. 276*, 22680−22684.
34. Tamamizu-Kato, S., Kosaraju, M. G., Kato, H., Raussens, V., Ruysschaert, J.-M., and Narayanaswami, V. (2006) Calcium-triggered membrane interaction of the α-synuclein acidic tail, *Biochemistry 45*, 10947−10956.
35. Cevc, G. (1990) Membrane electrostatics, *Biochim. Biophys. Acta 1031*, 311−382.
36. McLaughlin, S., Mulrine, N., Gresalfi, T., Vaio, G., and McLaughlin, A. (1981) Adsorption of divalent cations to bilayer membranes containing phosphatidylserine, *J. Gen. Physiol. 77*, 445−473.
37. Mayer, L. D., Hope, M. J., and Cullis, P. R. (1986) Vesicles of variable sizes produced by a rapid extrusion procedure, *Biochim. Biophys. Acta 858*, 161−168.
38. Greenfield, N., and Fasman, G. D. (1969) Computed circular dichroism spectra for the evaluation of protein conformation, *Biochemistry 8*, 4108−4116.
39. MacDonald, P. M., and Seelig, J. (1987) Calcium binding to mixed phosphatidylglycerol−phosphatidylcholine bilayers as studied by deuterium nuclear magnetic resonance, *Biochemistry 26*, 1231−1240.
40. Privalov, P. L. (1990) Cold denaturation of proteins, *Crit. Rev. Biochem. Mol. Biol. 25*, 281−305.
41. Korlach, J., Schwille, P., Webb, W. W., and Feigenson, G. W. (1999) Characterization of lipid bilayer phases by confocal microscopy and fluorescent correlation spectroscopy, *Proc. Natl. Acad. Sci. U.S.A. 96*, 8461−8466.
42. Epand, R. M., Shai, Y., Segrest, J. P., and Anantharamaiah, G. M. (1995) Mechanisms for the modulation of membrane bilayer properties by amphipathic helical peptides, *Biopolymers 37*, 319−338.
43. Ludtke, S., He, K., and Huang, H. (1995) Membrane thinning caused by magainin 2, *Biochemistry 34*, 16764−16769.
44. Matsuzaki, K. (1999) Why and how are peptide-lipid interactions utilized for self-defense? Magainins and tachyplesins as archetypes, *Biochim. Biophys. Acta 1462*, 1−10.
45. Ludtke, S. J., He, K., Heller, W. T., Harroun, T. A., Yang, L., and Huang, H. W. (1996) Membrane pores induced by magainin, *Biochemistry 35*, 13723−13728.
46. Basanez, G., Sharpe, J. C., Galanis, J., Brandt, T. B., Hardwick, J. M., and Zimmerberg, J. (2002) Bax-type apoptotic proteins porate pure lipid bilayers through a mechanism sensitive to intrinsic monolayer curvature, *J. Biol. Chem. 277*, 49360−49365.
47. Zakharov, S. D., Lindeberg, M., Griko, Y. V., Salamon, Z., Tollin, G., Prendergast, F. G., and Cramer, W. A. (1998) Membrane-bound state of the colicin E1 channel domain as an extended two-dimensional helical array, *Proc. Natl. Acad. Sci. U.S.A. 95*, 4282−4287.
48. McMahon, H. T., and Gallop, J. L. (2005) Membrane curvature and mechanisms of dynamic cell membrane remodelling, *Nature 438*, 590−596.
49. Andersen, O. S., and Koeppe, R. E. I. (2007) Bilayer thickness and membrane protein function: an energetic perspective, *Annu. Rev. Biophys. Biomol. Struct. 36*, 107−130.
50. Zakharov, S. D., Rokitskaya, T. I., Shapovalov, V. L., Antonenko, Y. N., and Cramer, W. A. (2002) Tuning the membrane surface potential for efficient toxin import, *Proc. Natl. Acad. Sci. U.S.A. 99*, 8654−8659.
51. Yamaji-Hasegawa, A., and Tsujimoto, M. (2006) Asymmetric distribution of phospholipids in biomembranes, *Biol. Pharm. Bull. 29*, 1547−1553.
52. Balasubramanian, K., and Schroit, A. J. (2003) Aminophospholipid asymmetry: a matter of life and death, *Annu. Rev. Physiol. 65*, 701−734.
53. Martin, E. D., Gonzalez-Garcia, C., Milan, M., Farinas, I., and Cena, V. (2004) Stressor-related impairment of synaptic transmission in hippocampal slices from α-synuclein knockout mice, *Eur. J. Neurosci. 20*, 3085−3091.
54. Rosenmund, C., Rettig, J., and Brose, N. (2003) Molecular mechanisms of active zone function, *Curr. Opin. Neurobiol. 13*, 509−519.
55. Atlas, D. (2001) Functional and physical coupling of voltage-sensitive calcium channels with exocytotic proteins: ramifications for the secretion mechanism, *J. Neurochem. 77*, 972−985.
56. Lee, H. J., Patel, S., and Lee, S. J. (2005) Intravesicular localization and exocytosis of α-synuclein and its aggregates, *J. Neurosci. 25*, 6016−6024.

57. Sung, J. Y., Park, S. M., Lee, C. H., Umm, J. W., Lee, H. J., Kim, J., Oh, Y. J., Lee, S. T., Paik, S. R., and Chung, K. C. (2005) Proteolytic cleavage of extracellular secreted α-synuclein via matrix metalloproteinase, *J. Biol. Chem. 280*, 25216−25224.
58. Zhang, W., Wang, T., Pei, Z., Miller, D. S., Wu, X., Block, M. L., Wilson, B., Zhang, W., Zhou, Y., Hong, J. S., and Zhang, J. (2005) Aggregated α-synuclein activates microglia: a process leading to disease progression in Parkinson's disease, *FASEB J. 19*, 533−542.
59. Zakharov, S. D., Kotova, E. A., Antonenko, Y. N., and Cramer, W. A. (2004) On the role of lipid in colicin pore formation, *Biochim. Biophys. Acta 1666*, 239−249.

BI701275P